Nuclear Instruments and Methods in Physics Research A 332 (1993) 395–412
North-Holland

NUCLEAR INSTRUMENTS & METHODS IN PHYSICS RESEARCH
Section A

A three-ton liquid argon time projection chamber

P. Benetti [f], A. Bettini [e], E. Calligarich [f], F. Casagrande [e], P. Casoli [e], F. Cavanna [c], P. Cennini [a], S. Centro [e], M. Cheng [d], S. Cittolin [a], D. Cline [d], B. Dainese [e], C. De Vecchi [e], R. Dolfini [f], L. Fortson [b], F. Gasparini [e], A. Gigli Berzolari [f], F. Mauri [f], L. Mazzone [f], C. Montanari [f], G. Muratori [e], S. Otwinowski [d], A. Pepato [e], L. Periale [g], G. Piano Mortari [c], A. Piazzoli [f], P. Picchi [b], F. Pietropaolo [e], A. Rappoldi [f], G.L. Raselli [f], P. Rossi [e], C. Rubbia [a], D. Scannicchio [f], S. Suzuki [e], S. Ventura [e], H. Wang [b] and M. Zhou [d]

[a] *CERN, CH-1211, Geneva 23, Switzerland*
[b] *Lab. Naz. di Frascati dell'INFN, via E.Fermi 40, Frascati (Roma), Italy*
[c] *Dipartimento di Fisica e INFN, Università dell'Aquila, via Vetoio, Coppito (AQ), Italy*
[d] *Department of Physics, UCLA, Los Angeles, CA 90024, USA*
[e] *Dipartimento di Fisica e INFN, Università di Padova, via Marzolo 8, Padova, Italy*
[f] *Dipartimento di Fisica e INFN, Università di Pavia, via Bassi 6, Pavia, Italy*
[g] *ICGF del CNR di Torino, corso Fiume 4, Torino, Italy*

Received 29 January 1993

We have constructed and operated a 3 ton liquid argon time projection chamber for the R&D programme of the ICARUS project. The chamber has been in operation since May 1991 collecting events from cosmic rays and a monochromatic gamma ray source. We describe the construction of the different detector components and their assembly; we report the solutions found to the major technological problems and the operation of the detector. The detector can be built in large masses and is continually sensitive providing bubble chamber quality images of ionising events; some examples will be shown. The energy resolution is a few per cents in the MeV region. The space resolution is of the order of 100 μm. The novel technique we have developed provides a basis for building superior detectors in underground and accelerator experiments.

1. Introduction

The role of bubble chambers in elementary particle physics has been of fundamental importance due to their capability to give high resolution, unbiased, three dimensional images of ionising events. Bubble chambers can accomplish simultaneously the two basic functions of target and detector, due to the high density of the liquid medium. This characteristic has been essential for a number of experiments. Electronic detectors, contrary to bubble chambers, can be triggered and read out at fast rates. They replaced the bubble chambers for this reason. Due to the low density of the gaseous medium they employ, the target and detector functions must be separated. This separation is a drawback for a class of experiments looking for rare contained events, e.g., proton decay and neutrino interactions. The ideal detector for these applications would be a liquid detector with high spatial resolution and electronic readout (the electronic bubble chamber).

A precise proposal, the liquid argon time projection chamber (LAr-TPC), was made by Rubbia in 1977 [1]. The detector is continually sensitive, self-triggering and able to provide three dimensional images of any ionising event as an electronic bubble chamber. Particle identification is available by measuring the ionisation charge per unit length (proportional to dE/dx) and the range of the stopping particles. The detector is also a superb calorimeter of very fine granularity and high accuracy. The ICARUS collaboration proposed [2] in 1985 a multi-kiloton LAr TPC to be run in the Gran Sasso Laboratory to search for rare underground phenomena ranging from proton decay to real time solar neutrino observations, as well as neutrino oscillations and relic supernovae's neutrinos.

A brief description of the operating principles of the liquid argon (or other cryogenic liquid) TPC follows. Simple techniques have been developed [3,4] to obtain liquid argon at a level of purification (< 1 ppb of O_2 equivalent) such that free electrons, as those produced by an ionising event, can drift over distances of several metres. Any ionising event taking place in a volume of several cubic metres of ultra pure LAr, where a uniform electric field is applied, will produce

0168-9002/93/$06.00 © 1993 – Elsevier Science Publishers B.V. All rights reserved

ion–electron pairs. A fraction of them, dependent on the field intensity and the density of ion pairs, will not recombine and will immediately start to drift parallel to the field in opposite directions. The motion of both the electrons and the ions induces a current on any electrode present in the volume or around it. The current intensity is proportional both to the flux of the electric field across the electrode due to the drifting charge and to the speed of the charge. The speed of the electrons is five orders of magnitude greater than that of the ions therefore only electrons give an appreciable contribution to the induced current.

No amplification is present in the liquid medium near the wires. This has an advantage and a disadvantage. The disadvantage is that the ionisation charge to be detected is extremely small. Typically 8000 electrons per mm are produced by a minimum ionising particle and a large fraction of these recombines, especially at low field intensities. The problem can be solved with low noise FETs that have been commercially available for the past few years. The advantage is that the drifting electrons can be used many times to induce signals on different wire planes. This allows a three dimensional read-out as proposed by Gatti et al. [5]. In practice the read-out is performed with a chamber consisting of a number of parallel wire planes located at the end of the sensitive volume (assuming the drift direction pointing to the end). We call z the coordinate along the electric field with x and y the coordinates on the plane of the chamber. The absolute z coordinate is given by a measurement of the drift time, provided that the $t = 0$ time and drift speed are known. The drifting electrons reach and cross in sequence the following wire planes: 1) a plane of wires running, e.g., in the y direction, functioning as the screening grid; 2) a plane of wires running again, e.g., in the y direction, located at a distance of some mms below the screening grid where its function is to measure the x coordinate; 3) a plane of wires running in the x direction, located at a distance of some mms below the previous plane; its function is to measure the y coordinate. The electric field intensities in the sensitive volume above the screen grid and in the gaps between the grids must be arranged to have a complete transparency of the grids.

The sequence of wire planes can continue if more coordinates are needed and the angles between wire directions can be chosen at will. For our prototype detectors we have chosen two orthogonal coordinates (x and y) as described above; we have chosen the wire pitch and the distance between the planes to be 2 mm to have the best possible spatial granularity. Our 3D pixel (our "bubble") is a 2 mm per side cube. The last grid need not be transparent; we use it to finally collect the drifting electrons.

An electron drifting in the sensitive volume above the screen grid does not give any current in the coordinate planes (in the case of perfect shielding). A positive induced current starts in the x coordinate plane when the electron crosses the screen grid, becomes negative when the electron crosses the coordinate plane and ends when the electron crosses the y coordinate plane. We call the x coordinate plane the "induction plane". The current on the y coordinate plane has similar behaviour, with the exception that only the positive current is present; when the electrons reach the plane they fall on the wires. We call this plane the "collection plane". We integrate the current from each wire of the coordinate planes and sample the charge with flash ADCs at a frequency that provides several measurements for each pulse.

We built and operated in a 5 GeV pion beam a small LAr TPC to make preliminary tests of the basic technological points after having optimised the geometry of the chamber planes by computation of the field and simulation of the signals. The maximum drift distance was 24 cm; the chamber had a screening grid and a single coordinate plane with an 8×8 cm^2 area; the geometry is shown in fig. 4. The results have been published elsewhere [6–8]. Here we simply summarise the most important ones:

1) ultra-high purity liquid argon can be easily obtained using commercial Oxisorb [9] cartridges and molecular sieves along with high vacuum components and procedures. Free electron lifetimes in the range of several milliseconds were routinely obtained corresponding to potential drift distances of metres.

2) we obtained very neat images of ionising events operating the single plane both in the induction mode and in the collection mode.

3) we observed the effect of the diffusion and of the field dependence of the free electron yield and found them to be in agreement with theory.

4) we evaluated the energy resolution in the MeV region and found it to be very good (of some per cent) in agreement with the measurements of other groups [10].

5) we measured the space resolution in the drift coordinate to be 60 μm for 5 GeV tracks.

The ICARUS research program is very complex and ambitious and cannot be realised in one step since it involves the introduction on a large scale of several innovative technologies. After obtaining the important results we have just mentioned, in 1989 we organised the ICARUS program to follow a series of steps: 1) an initial phase of research and development, 2) the construction and operation of a detector of approximately 200 tons for solar neutrino studies [11] (ICARUS1) and 3) the final multi-kiloton detector.

Step 1 is an intensive R&D programme on a reasonable scale prototype detector aiming to solve the main technological problems:

a) the liquid argon must be kept ultra pure even in the presence of a large number of feedthroughs for the signals and the high voltage and with wire chambers, cables, etc. in the clean volume. The contamination by electronegative molecules must be kept to around 0.1 ppb to allow drifts on long distances (metres) without capture of the ionisation electrons;

b) all the materials employed in the construction of the detector must be extremely clean and non degassing and the feedthroughs between pure argon and the outside world must be completely tight to avoid contamination due to leaks;

c) the wire chambers must be able to perform the non destructive read-out with several wire planes with a few mm pitch; they must be built out of non contaminating materials and must stand the thermal stress going from room to liquid argon temperatures; the precision and the reliability of the mechanics must be high and a good knowledge of the electric field in the detector must be granted;

d) low noise preamplifiers to get a good signal to noise ratio must be developed. It must be remembered that we work with no amplification in the liquid; the signal is very small, of the order of 10000 electrons for a minimum ionising track in a 2 mm wire pitch;

e) given the large amount of digitisations of the three-dimensional image, software architectures and algorithms must be developed for data reduction.

To study these points, we decided to build a prototype detector with a sensitive mass of two tons (total Ar mass is about three tons) corresponding to about 1/100 of that of the ICARUS1 detector. In designing the different components of the prototype we constantly had to be aware that the technical solutions must be appropriate for the final detector. The three ton prototype detector has been taking data for one and a half years. We will describe here its main characteristics, its behaviour and the principal conclusions we can draw from our experience. Preliminary results have been reported elsewhere [8,12], detailed discussions on the measurements performed with the detector will be reported in a following paper.

The paper is organised as follows: in section 2 through 5 we describe the mechanics of the dewar, the electrodes and the wire chambers along with the related cleaning procedures, in section 6 the purification system and the purity monitor are described, in section 7 we discuss the internal low capacitance cables, in section 8 the signal and the high voltage feedthroughs, in section 9 the analogue and digital electronics, in section 10 the readout organisation and the filtering algorithms. We will then report some results of the operation of the detector and show examples of cosmic ray events and of low energy events induced by a radioactive source. Finally, in section 12 we will draw conclusions.

2. Mechanics of the dewar

The cryostat, shown schematically in fig. 1, consists of two coaxial vertical stainless steel (AISI 304L) vessels [13]. The shape of both the external (1 in fig. 1) and the internal (2) vessels is a cylinder with hemispherical bottoms. The two cylinders are connected by an annular flange (3 in fig. 1) on the top of the dewar. Another circular flange [14] (4) hermetically seals the inner volume of the dewar; this flange hosts the feedthroughs for the signal and the high voltage (7) cables, those for the argon circulation pipes and for all the necessary services (pressure metres, liquid argon level indicators, thermometers, etc.). The outer vessel has a diameter of 1.5 m, a height of 3.3 m and a wall thickness of 3 mm. The inner vessel has a diameter of 1.05 m, a height of 3.08 m and a wall thickness of 3 mm. The total internal volume is 2.61 m^3.

The preamplifiers must be located as close as possible to the signal feedthroughs to reduce to a minimum the input capacitance and hence the noise. They are hosted in eight cylindrical boxes (8) connected with tubes to the upper flange (only two out of eight are shown in fig. 1). The tubes are bent for lack of space. The boxes are refrigerated by Peltier valves at the

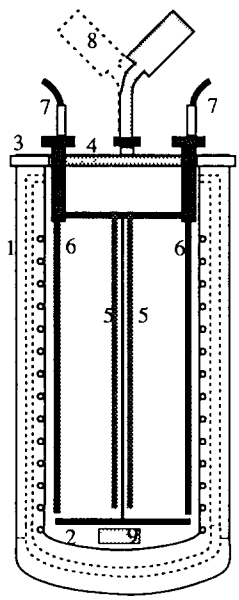

Fig. 1. Schematic view of the mechanics of the detector. 1 is the outer vessel, 2 the inner vessel, 3 the annular flange, 4 the circular flange, 5 the wire chambers, 6 the cathodes, 7 the high voltage feedthroughs, 8 the boxes containing the preamplifiers (two out of eight shown), 9 the purity monitor.

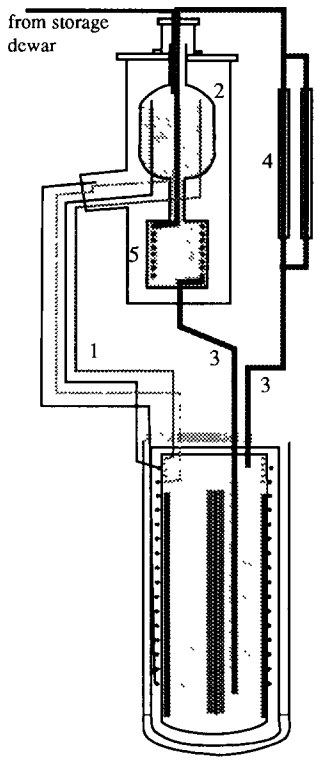

Fig. 2. The cryogenic system shown enlarged with respect to the dewar. 1 are the pipes used for cool down and continuous cooling, 2 is the 40 l dump tank, 3 are the pipes for ultra pure argon recirculation, 4 is the purification system, 5 the condensation system.

optimum temperature. The signal feedthroughs are flushed with cold nitrogen gas to keep them in a dry environment to reduce the risk of discharges.

The evacuated volume (10^{-3} mbar obtained with a rotative pump) between the two vessels is filled with a super-insulator, consisting of two copper screens (shown dotted in fig. 1) surrounding completely the inner vessel, wrapped with several layers of aluminised mylar sheets.

The cryogenic system of the detector has to perform four functions: i) cool-down of the inner vessel before filling with pure liquid argon; ii) continuous cooling of the liquid argon during operation of the chamber for extended periods of time; iii) recirculation and continuous purification of a fraction of the argon to eliminate possible contamination; iv) warm-up of the inner vessel before emptying the liquid argon.

The cryogenic system consists of the following components illustrated in fig. 2. The liquid argon for cooling is supplied by a dump tank of 40 l in volume (2 in fig. 2) situated above the cryostat. This tank can feed by gravity the copper serpentine surrounding the cryostat. An argon storage dewar fills the dump tank automatically three times per day. A level indicator coupled with an electromagnetic valve controls the filling of the tank. Filling starts when the level falls below some pre-set value and stops automatically when the tank is full.

The consumption of cooling argon is 4–5 l per hour when the inner vessel is full of pure liquid argon at 87 K. The cooling of the inner vessel can be performed by liquid argon circulating in a copper serpentine coiled around the vessel.

The ultra pure liquid argon in the dewar even in absence of any leak, can be contaminated by outgassing of the walls and of the various materials (electrodes, chambers, spacers, cables, high-voltage resistors, etc.) contained in the dewar. In practice, as it will be discussed below, the main outgassing sources are the parts of the system that are not in direct contact with the liquid and have as a consequence higher temperatures. The closing flange and the signal cables in particular have large surfaces in the clean volume at almost room temperature and are the main source of outgassing. To keep the liquid argon at the necessary purity we have provided a recirculation system. The naturally evaporating argon is brought through a pipe (3 in fig. 2) to a purification system (4 in fig. 2) similar to the main one that will be described in section 6, but with two Oxisorb/Hydrosorb cartridges in parallel to decrease impedance. The argon is then recondensed in a serpentine (5) in the 40 l tank. The hydraulic circuit just described is ultra-clean. As we will show, the recirculation system proved to be an essential part of the apparatus necessary to maintain the purity of the argon. In case of failure of the cooling system, the liquid argon inside the cryostat will be vented through a rupture disc rated at about 2 bar absolute and eventually through the pumping system previously described.

3. The configuration of the inner electrodes

Because this prototype should be used also to test the feasibility of the technological solutions to be adopted in ICARUS1, the internal configuration of this dewar should follow very closely the one proposed for the 200 ton detector.

The inner volume of the dewar is split into two independent semi cylindrical sections (each one a mirror image of the other) by means of a stainless steel septum put vertically along a diameter of the dewar. This septum is held in position between two horizontal circular metal plates. These plates (one at the top and one at the bottom) and the central septum form a solid structure independent of the surrounding dewar in which we insert the elements of the detector. The structure is suspended from the upper flange by means

of four rods. A small part at the top of the volume is excluded from this sectioning because it is needed as a service area to allow input/output for the electronics and high voltage for the detector sections and to monitor the liquid argon level.

Both sections are equipped with identical drift chamber systems (5 in fig. 1). Each wire chamber covers a surface equal to 2.4×0.9 m^2 and is supported by frames on each side of the central septum. The drift volume is defined by the chamber itself, a system of "race-tracks" [14] consisting of ten tubular rods of 2 cm in diameter (not shown in fig. 1) and a cathode. The race-track rings are separated from each other by 5 cm; their distance from the wall of the dewar is at least 5 cm. The race-track system is connected to the high-voltage power supply with each ring set at the appropriate voltage by means of a resistor chain. We use specially designed, thick film resistors finished with glass. Values range between 50 and 100 MΩ.

The purpose of the race-track system is to establish a well defined and uniform electric field over the entire detection volume so that the electrons may be correctly and efficiently drifted onto the wire plane.

The cathode is a vertical metal plate (6 in fig. 1) 2 cm thick, 30 cm wide and 2.4 m high, at a negative voltage of 45 kV maximum. The distance between cathode and wire chamber is 42 cm (maximum drift distance). The maximum electric field in the drift volume is then 1 kV/cm. Fig. 3 represents the electric field configuration in a horizontal cross-section of the dewar volume. The wire chambers, the race-tracks and the cathodes are also shown.

The high voltage power supply can deliver a maximum voltage of 150 kV, stable within 10^{-5}, and a maximum current of 0.5 mA. It is connected to the high voltage cable through a 10 MΩ resistor that, associated with the cable capacitance (1.5 nF), is used as a filter. Under these conditions no additional noise due to the high voltage ripple is observed at the sense wires. The total useful volume for signal detection is equal to 1.45 m^3 corresponding to 2 tons of liquid argon.

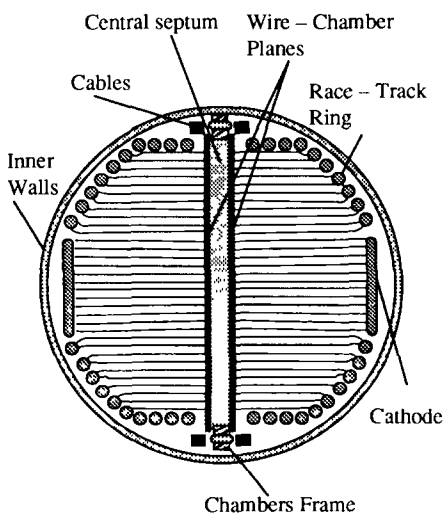

Fig. 3. Top view of the field lines in the drift region.

4. Cleaning of the components

Cleanliness of the internal vessel and of all the components in the dewar is of primary importance in preserving the purity of the liquid argon. The main operations we performed on the dewar were: degreasing by a bath of water with detergent at 50°C excited by ultrasounds, washing with demineralised water (at 90°C), drying and thermal outgassing by means of hot (80°C) water circulating in the serpentine, while evacuating the dewar with a two stage LEYBOLD [15] pumping system. It consisted in a primary rotative pump (type D40B, speed 40 m^3/h, max vacuum 10^{-4} mbar) followed by a liquid nitrogen cold trap, to avoid back-diffusion of mechanical oil, and in a magnetic, oil-free, turbo-molecular pump (type TURBOVAC 340M, speed 300 l/s, max vacuum $\approx 10^{-8}$ mbar) directly connected onto the dewar through a DN 100 flange. The pressure and the residual gas composition were continually checked by means of a mass spectrometer (LEYBOLD type QUADRUVAC PGA 100) also connected on the top flange of the dewar. Following a similar procedure in the tests made with the small scale chambers, we had reached a degassing rate at room temperature of 10^{-12} mbar 1 cm^{-2} s^{-1} compatible with what we expected from stainless steel surfaces and found it to be perfectly adequate for ultra pure argon. After two weeks of bake-out we reached a residual pressure at room temperature of 5×10^{-8} mbar and a total degassing rate of 1.5×10^{-11} mbar/s corresponding again to a specific degassing rate of 3.3×10^{-12} mbar 1 cm^{-2} s^{-1}.

We then opened the flange and introduced all the detector elements as well as the necessary probes. The bake-out was performed again by circulating water at 80°C in the serpentines with purified Ar gas now in the dewar to have thermal contact between the walls and internal parts. After two weeks, the residual pressure in the evacuated dewar was 5×10^{-8} mbar at room temperature and the total degassing rate was 3×10^{-9} mbar/s. This value is more than two orders of magnitude bigger than that reached with the empty dewar; the increase is due to the large surfaces of the detector elements (mainly the chambers and the cables) and the higher outgassing rate from the kapton surfaces of the cables. When the system is in operation, most of these materials are at liquid argon temperature and then the

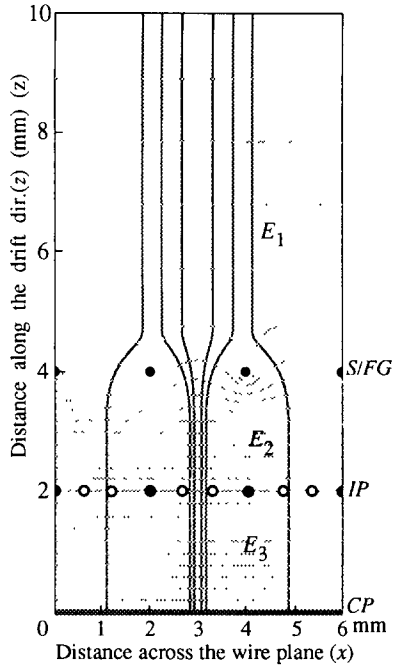

Fig. 4. The electric field map near the wire chambers. S/FG is the screening/focusing grid, IP and CP the induction and collection planes respectively. In the induction plane sense wires are open circles, screen wires closed circles.

degassing rate is reduced. We then decided to start the filling operations.

5. Mechanics of the chambers

There are two wire chambers on each side of the central septum. Each chamber consists of three planes of wires. As mentioned in the introduction, going from outside to inside, the first plane is a screening/focusing grid followed by the induction plane and finally by the collection plane.

We have studied the geometry of the wire planes both by simulation and by construction and operation of a prototype LAr TPC. The results have been published in [7] where the optimised geometry is fully discussed.

We only recall here that the induction plane is made by doublets of sense-wires (each doublet is read-out by one amplifier) separated by 0.6 mm; the centres of two adjacent doublets are separated by 2 mm and there is a screen wire between them. The ratio of the electric fields above the screening grid (E_1) and between it and the induction plane (E_2) is chosen to focalise the field lines in between the two sense wires of the doublet as shown in fig. 4. This geometry has two advantages: i) the charge induced by a drifting electron is almost independent of its position in the drift cell and ii) an electron drifting in one cell induces only a small fraction ($< 6\%$) of the total charge in the contiguous cells. The collection plane is made of sense wires at a 2 mm pitch separated by screen wires. The fields above (E_2) and below (E_3) the induction plane are chosen to assure complete transparency of the induction plane. The condition on the three field intensities is: $E_3 = E_2 = 5\ E_1$.

The wires (stainless steel, 100 μm in diameter) are kept in position and under tension on the frame of the chamber by a structure made out of MACOR [16] bars. They are held by small conical tubes crimped around them while the tubes are held in turn by the holes drilled in the MACOR bar. Their diameter is 150 μm. In the case of the doublets of the induction plane we insert both wires in the same tube (300 μm in diameter). The complicated structure and the closeness (0.6 and 0.7 mm in the induction plane, 1 mm in the collection plane) of the adjacent wires forced us to drill two different rows in the MACOR bars. The wires then pass over combs to assure their correct position, as shown in fig. 5 for the induction. MACOR combs are also used every 80 cm in the induction plane, where the wires are longer, to reduce the gravitational sag as well as the electrical instability.

The wires of the collection plane are strung at 500 g, those of the induction plane at 750 g. Wires and tubes were cleaned in acetone, alcohol and hexane baths excited by ultrasound. Each drift volume has a total of 1800 vertical wires (2.4 m long) of which 900 are sense-wires (corresponding to 450 pairs). The collection plane consists of a total of 2400 horizontal wires (0.9 m long) of which 1200 are sense-wires.

A wire stretching apparatus was designed and built for the assembly of the two chambers. It is composed of the following items: a trolley taking the wires from one side of the chamber to the other, a piston to define the tension of the wire that consists of some brass weights suspended in dynamic equilibrium on a compressed air cushion and a movable hydraulic flipper to crimp the wire in the copper tube. The tension of each

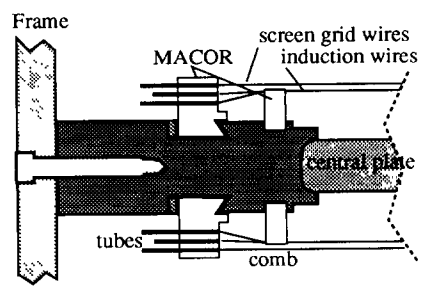

Fig. 5. Detail of the macor pieces holding the wires of the screen grid and induction planes.

wire was checked both on line and after completion of the chamber by inducing resonant conditions in the wire.

The total number of sense-wires (collection plus induction) for the two drift chambers of the detector is 3300. Unfortunately, the surface available for the corresponding feedthroughs is not enough even with the special design described in section 8. For this reason, we decided to connect electrically together each horizontal sense-wire of one chamber with the corresponding one of the other chamber. The reduced number of feedthroughs (2100) could then be placed more easily on the available area. The final cleaning of the chamber was performed with separate baths of acetone, methanol and hexane; the system was then assembled in a clean room.

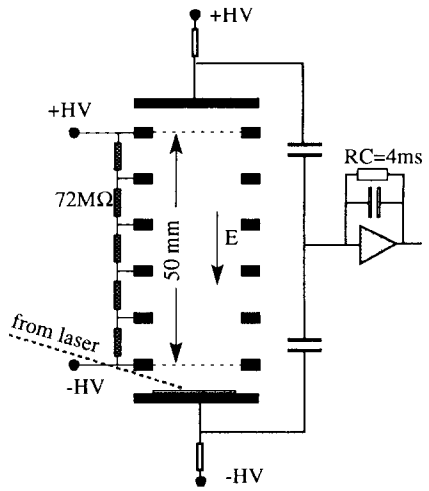

Fig. 7. Schematic view of the purity monitor.

6. Purification system

The purification system design is based on a systematic study made previously. The contribution to the purification process of different commonly used elements was systematically investigated. The results are published elsewhere [8]. The adopted configuration is shown schematically in fig. 6. It is constructed using two industrial high flux (100 m^3/h at NTP) cartridges from Messer Griesheim, modified substituting the original flanges with ConFlat type [17] ones to allow high vacuum treatment. The first cartridge is HYDROSORB [18] (a mixture of molecular sieves 5A and 13X) where its principal effect is to remove hydrocarbons by physical absorption. The second cartridge is OXISORB [18] used mainly to remove oxygen. All the components of the system are of ultra high vacuum grade. Valves are from NUPRO [19] or VAT [20], flanges are of the ConFlat type with copper gaskets.

All the components of the system are preliminarily cleaned following the procedures developed at CERN for the high vacuum LEP components; the system is baked under vacuum (10^{-7} mbar) at 200°C. The new OXISORB and HYDROSORB cartridges are always purged by flushing through them some hundred litres of Ar.

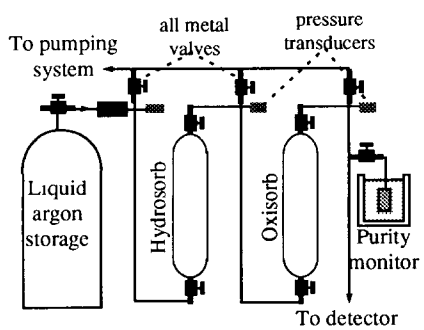

Fig. 6. Schematic view of the purification system.

We use commercial liquid argon as input to the purification system. After evaporation, the Ar gas goes through the two cartridges and to the final destination. In parallel with the pipe to the detector dewar, we can fill a monitor chamber to measure the free electron lifetime. During the filling of the detector vessel the flux through the purifier was 7000 l/h (NTP). The free electron lifetime was checked periodically and always found at the limits of the sensitivity of the monitor, i.e. several milliseconds long.

The monitor chambers we use for measuring and controlling the electron lifetime (a second one is on the bottom of the detector dewar) have been described elsewhere [8]. We only recall here that the monitor is a doubly grided ionisation chamber, shown schematically in fig. 7. The anode and cathode are almost completely screened by two grids located 1 cm from each electrode. The field intensities are chosen to insure complete transparency of the grids. The two grids are separated by a 5 cm long drift space. Basically we measure the attenuation due to electronegative impurities of an electron cloud drifting over this distance by comparing the charge leaving the cathode to that reaching the anode.

The currents from the cathode and the anode feed the same integrating amplifier. Free electrons are produced by a short (20 ns) UV (266 nm wavelength) laser pulse brought to a gold deposit on the copper cathode through an optical fibre. The electron cloud photo-produced by the light pulse drifts initially to the first grid producing a positive current in the amplifier. This current vanishes in the instant the electrons cross the cathode grid. The charge integrated by the amplifier is then equal to the charge Q_c produced at the cathode.

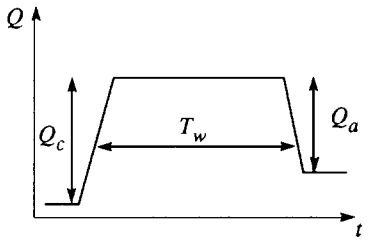

Fig. 8. The charge pulse of the purity monitor.

While the charge drifts in the uniform field between the two grids, no current is seen by the amplifier. If electronegative impurities are present, its value diminishes. When the charge finally crosses the anode grid it produces a negative current in the input of the amplifier and a negative step in the output (charge) signal; the height of the step is equal to the surviving charge (Q_a) reaching the anode (see fig. 8). As shown in reference [8], if T_w is the drift time and τ the free electron lifetime, we have simply: $Q_a/Q_c = \exp(-T_w/\tau)$. Obviously the sensitivity is higher for longer drift times, which can be obtained by working with low electric field intensities. The minimum practical field intensity is 50 V/cm corresponding to a maximum measurable lifetime of 2–3 ms.

7. Internal cables

As mentioned before, there is no charge amplification at the wires in a liquid argon TPC. As a consequence the charge signal is very small, typically between one and two femtocoulomb for a 2 mm pitch (or between 6000 and 12000 electrons). The equivalent noise charge (ENC) from the preamplifiers must be reduced to the physically allowed minimum. The main contribution comes from series noise that is proportional to the input capacitance of the amplifiers located immediately outside the upper flange of the dewar. The input capacitance is the sum of the sense wire capacitance and of the capacitance of the connecting cable. The latter must be reduced as possible. The capacitance per unit length is 30 pF/m for the sense wire doublets of the induction plane, corresponding to a total capacitance (2.4 m length) of 72 pF. The capacitance per unit length of the collection wires is 20 pF/m corresponding to a total capacitance (two together of 0.9 m length) of 36 pF.

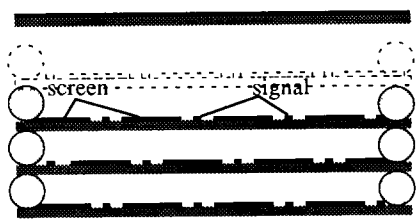

Fig. 9. Schematic view (not on scale) of a section of the stack cable showing the kapton layers, the copper signal and screen strips and the teflon spacers.

In summary, the specifications of the cables are: the capacitance per unit length must be a minimum, the cross talk amongst channels must be as low as possible and the materials used should not contaminate the ultra pure argon.

The cable we finally developed is schematically shown in fig. 9. The basic element is a metallised (18 μm Cu) Kapton flexible printed circuit (75 μm thick); it contains 8 signal strips (127 μm wide) interleaved with 9 screen strips (3500 μm wide) that are connected with the sense wires and the screen wires respectively. A cable stack is made overlapping 32 printed circuits for a total of 256 channels. The printed circuits are separated by 1.5 mm diameter teflon spacers as shown in fig. 9. Contiguous printed circuits in the stack are staggered by half a period to assure the best screening of the channel strips. The last (upper) flat cable in the stack is made of a continuous screen layer. A female connector is clamped at the end of each flat cable with the pitch matching the pitch of the pins on the feedthroughs.

The capacitance per unit length is low (40 pF/m) giving a total capacitance of the 3.5 m long cables of 140 pF and the cross-capacitance is $< 2\%$. The materials are known to be non-contaminant and are easy to clean. On the other hand, there are difficulties in producing long cables and in keeping the layers separate. Each cable-stack follows a vertical frame of the chamber and goes to a feedthrough matrix (one for each cable stack), through the upper service area.

8. Feedthroughs

As mentioned in section 5 we have a total of 2100 signal wires that must reach the amplifiers located outside the detector dewar. We also need two feedthroughs for the 45 kV potential of the cathodes for the two semi-cylindrical sectors. We will describe now the two types of feedthroughs.

Signal feedthroughs. The problems to be solved in designing and building the signal feedthroughs are the following. The feedthroughs must be completely reliable; no one in the more than two thousand needed must leak. The space taken by each channel must be as small as possible, given the high total number and the limited space available on the upper flange. They must stand a moderately high voltage (1.5 kV) with respect to ground. The materials used should not contaminate the ultra-pure argon. The cost must be as low as possible.

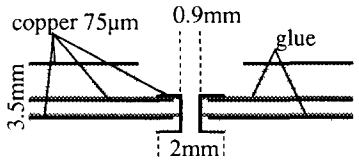

Fig. 10. Schematic view of one of the signal feed through holes in the printed circuit.

After a series of tests, the following solution was adopted. For each cable stack containing 256 signal strips plus screen strips a feedthrough matrix is provided. Each matrix contains a total of 350 feedthroughs and is located on the upper flange in correspondence of one of the eight tubes going to one box containing the preamplifiers.

The matrices are made with the printed circuit board technique. Each of them is one sandwich of one 1.6 mm and two 0.8 mm thick FR4 epoxy foils pierced by metallised holes as shown schematically in fig. 10. The matrix contains 35 rows of 10 holes each at a 2.54 mm pitch; the distance between two rows is 1.27 mm. Pins are soldered in the holes to ensure vacuum tightness. The two lateral pins in each row are used for the screen strips, while the central 8 are used for the signal strips of each flat kapton cable. After soldering, the plate with the pins is washed in separate baths of acetone, alcohol and hexane excited by ultrasound.

Each plate is tested for vacuum tightness and for electrical insulation, verifying that pins can stand a maximum potential difference of 1.5 kV between them and also to ground. The vacuum between the plate and the dewar flange is assured by an indium gasket. fig. 11 is a schematic representation of the electrical connections showing the resistors to the voltage supply, the blocking capacitors and the preamplifiers (sense wires and screening wires are brought to the same potential to avoid discharges and microphonic noise).

High voltage feedthroughs. Their specifications are the following. They must keep up to 45 kV with respect to ground; they must stand the temperature difference between room temperature and 87 K of the liquid argon; humidity condensations and frost formation must be avoided; only non contaminant material must

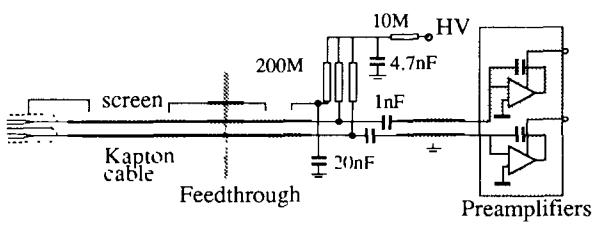

Fig. 11. Schematic view of the electrical connections of sense and screen wires.

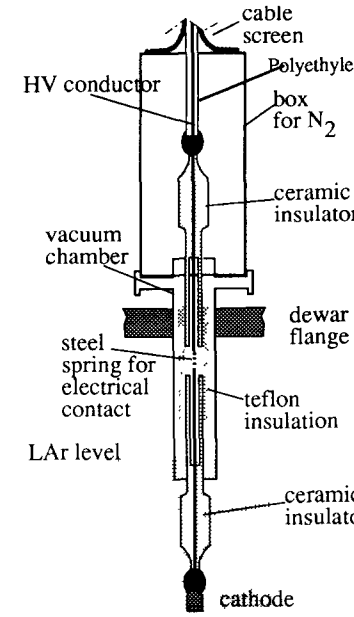

Fig. 12. Schematic view of the HV feedthrough.

be used. After a series of tests, the solution shown schematically in fig. 12 was adopted. The cable from the high voltage supply first penetrates a stainless steel box containing dry N_2 to avoid frost. The ground screen of the cable is terminated on the outside wall of the box; the copper conductor and the polyethylene insulator of the cable enter the box. Inside the box the conductor is terminated with an almost spherical stainless steel piece that is in contact with a stainless steel bar contained in a ceramic insulator. The lower part of the insulator is shaped as a tube and is contained in a second chamber, immediately following the box, were we keep a vacuum at a pressure less than 10^{-7} mbar.

The stainless steel bar ends in this box (to allow opening of the system) and is taken in safe electrical contact with a second similar steel bar contained in a second ceramic insulator by a stainless steel spring. The insulator leaves the vacuum chamber inside the dewar and the bar leaves the insulator inside the liquid argon, in a safe high electrostatic rigidity environment, and, through a second spheroidal steel piece, is connected to the cathode. The system has been tested for safety up to 100 kV.

9. Electronics

9.1. Analogue electronics

The analogue electronic chain is divided into three parts located in separate cabinets: the charge sensitive preamplifier and associated high voltage decoupling

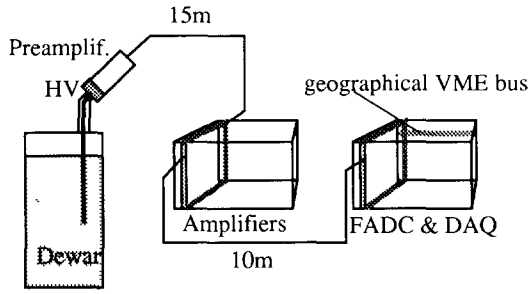

Fig. 13. Analogue electronics physical lay-out.

network, the amplifier/differential line driver and the line receiver/FADC driver as sketched in fig. 13.

The sense wires are connected to the analogue chain by the internal kapton cables and the feed-throughs described in the previous sections. On the high voltage decoupling network, sketched in fig. 14, the following functions are implemented: the high voltage distribution to the sense-wire and commons, the preamplifier input decoupling and the charge injection through a test capacitance. The network, serving eight sense-wires, is made on a ceramic hybrid circuit and is able to stand voltages up to 1.5 kV with leakage currents in the nanoampere region. The value of the resistors R is 200 MΩ and the decoupling capacitors $C_b = 1$ nF, 2 kV.

The calibration capacitances (C_t) are made using the ceramic as a dielectric and have a value of 3.5 pF ± 1.5%. As their accuracy is not good enough for calibration purposes, each capacitance on the hybrid is measured with a precision better than 0.5% and a calibration constant is associated with every sense-wire.

The preamplifier is made using the very well known j-FET input stage with unfolded cascode architecture [21]. Calculations made on the equivalent noise charge [22] demonstrate that in our detector the serial noise is dominant because of the rather high input detector capacitance (100 pF range).

The preamplifier schematics and its main characteristics are given in fig. 15. The actual circuit, made with hybrid technology, uses a single power supply of 12 V and a negative reference voltage of −7 V. The total power consumption is 100 mW. The circuit is a current integrator with a feed-back equivalent capacitance of

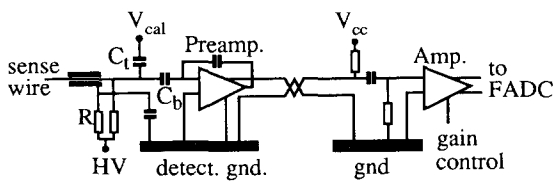

Fig. 14. Front end electronics.

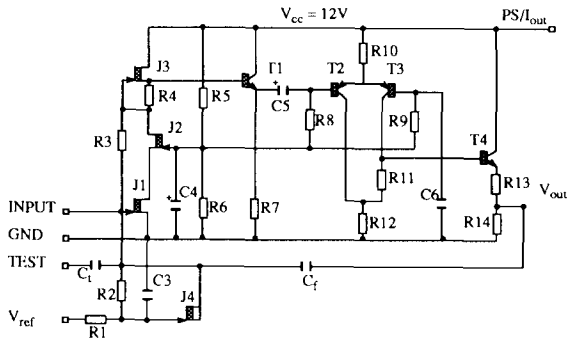

Fig. 15. Schematic of the preamplifier.

0.25 pF, a decay time-constant of about 0.5 ms and an equivalent input impedance of 200 Ω.

The input stage J1–J2 is a cascode made with two high transconductance j-FETs allowing good performance with respect to the serial noise. j-FET J3 is a current generator delivering a 5 mA current to the input stage. The following bipolar transistors (T1, T2, T3) act as a non inverting amplifier with a gain of ten. This increases the open loop gain hence reducing the input impedance. The output stage (T4), delivers a signal current of 8 μA/fC superimposed on the power supply DC current. The two currents share the same twisted-pair on each preamplifier avoiding any unexpected coupling between channels through the power supplies. This architecture presents the same advantages of a classical differential voltage transmission without the need of an additional differential output stage. We measured the noise of the amplification chain, shaping with a filter of the *CR–RC–RC* type (with a maximum at 2 μs) as a function of the input capacitance. The circuit shows a noise slope of 2.5 electrons per pF starting at 330 electrons at zero detector input capacitance.

Since the information to be digitised is the charge collected or induced on the sense-wire, the shaping is not implemented. Under these conditions the ENC is about 800 electrons for a 100 pF input capacitance representing a typical value for collection wires. The preamplifiers are mounted, in sets of 256 channels, inside water cooled Faraday cages. The amplifier section is based essentially on a commercial video amplifier with voltage gain control. Its output stage delivers (in differential mode on 120 Ω) a dc free signal of typically 18 mV/fC to the digitalisation board.

The FADCs are located on the data acquisition board. Their input line receivers are made with standard fast operational amplifiers having a DC coupled differential input on 120 Ω and a voltage gain of 5.45. Two additional single ended control inputs are implemented, the first to set the ADC pedestal over the entire range and the second to inject a fast test pulse.

The circuit uses the internal FADC reference to shift the DC input level to the voltage required by the FADC under all temperature conditions. The analogue chain gain is set to achieve a sensitivity of about 400 e/count corresponding to a signal of about 30 counts for the minimum collected charge.

9.2. The digital readout

The ICARUS detector readout system behaves as a large multichannel waveform recorder. It effectively stores the charge information collected by each sense wire during a time corresponding at least to the maximum drift time of the electrons (1.6 ms). The high resolution that has to be achieved, both in space and time sampling, brings the size of a single event to over hundreds of kbytes. The useful signal occupies only a small fraction of the data sample. Although in the initial phases of the experiment the complete information is useful for trouble shooting and debugging purposes, this is the real bottleneck of the whole data taking system, overloading both the on-line and off-line processing.

To improve performances in the future, the detector read-out will be divided into a number of subsystems with independent and identical read-out structures to increase the acquisition rate. The way to reduce the dimension of the event is to implement real time hardware solutions that will be able to detect valid data regions (amounting to only a few kilobytes) and save them on mass storage devices. Of course, this step can only be performed when the studies on the signal extraction algorithms will be consolidated.

All the digital electronics was custom designed for the ICARUS prototype having in mind the final large detector [23]. It is a VME-based system performing a full 1.6 ms long digitisation and recording of each signal from the analogue stage. The current signals coming from each of the sense-wires are analogically integrated and filtered as described in the previous paragraph. The charge output of the analogue stage is, for each channel, continually digitised and stored.

The digital conversion module, one for each channel, is a surface mounted module that consists of the following stages:

i) An analogue amplifying section which converts the differential input signal and perform the suitable scaling.

ii) An 8-bit FADC driven by a controllable speed clock. The clock speed can be chosen to be between 2.5 and 20 MHz. The full scale range is set to 300 mV, equivalent to a charge of 100000 electrons on the sense-wire. A DAC controlled baseline allows shifting of the zero level of the ADC to work properly with bipolar signals (e.g., to control the undershoot zero region of front end amplifiers). The 8-bit resolution bounds the maximum signal/noise ratio to 64 dB (quantization distortion). This fits our present needs as it is far over the actual analogue noise.

iii) An 8 Kbyte memory block. This memory can be subdivided in a number (from 2 to 16) of ring buffers; the FADC output cycles over one buffer switching to the next free one as a trigger comes. This procedure keeps the dead-time of the recording to a negligible level (below one clock period) as long as buffers are made free fast enough. Write access cycles are interlaced with read cycles, allowing random access to data from one buffer while running the acquisition on another buffer. The interlacing was chosen against dual port memories for cost reasons.

FADC modules are grouped by 16 on single boards (FM16); these boards fit on a VME-like crate (up to 20 boards on the same crate, giving 320 digital channels).

9.3. Board control and synchronisation

To simplify the drive and the synchronisation of the high number of ADCs, a parallel structure has been implemented at the crate level: one slot of each crate contains a module (RTX) which distributes the clock and drives the address lines common to the entire FADC set. As a result, all the FADCs in the crate are at any given time performing the same operation and all the sampled values are stored at the same relative address into the memory buffers.

The RTX module also provides an interface to a proprietary 50 lines bus which chains up to 8 crates to a VME interface (MANAGER). By means of sixteen VME registers supplied by the MANAGER, any VME master may select a specific RTX, set up acquisition parameters or read the memory contents of the specified channels. The memory content of the selected channel is mapped to the standard VME address space; a read request in that address space will be dispatched by the manager through the proprietary bus and acknowledged as the RTX returns the value.

10. Data acquisition and data filtering

Functional overview. The protocol to control the digitiser behaviour is based on a two FIFO queue structure for each RTX. To start acquisition, at least one entry must be submitted to the first queue (FIFO A) which contains the buffers that are available for writing. When a trigger comes, an entry is created on the second queue (FIFO B) reporting the trigger absolute time and the starting point in the ring buffer. The next free buffer, if any, is popped from the FIFO A to continue the acquisition. As long as the event process-

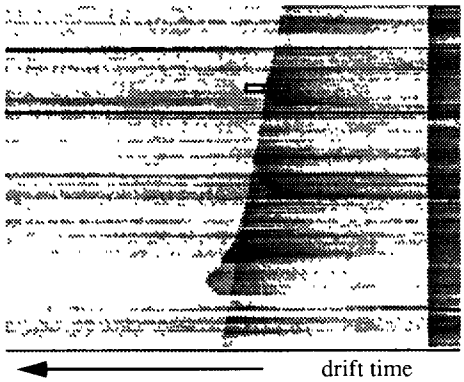

Fig. 16. The collection image of a cosmic ray track before filtering.

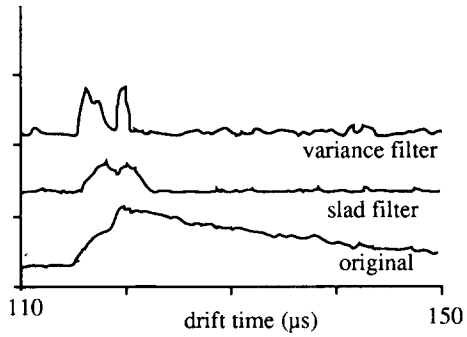

Fig. 17. The signal from the wire in the point marked with a rectangle in fig. 16 as digitised (original) and after filtering by the two algorithms described in the text.

ing software frees buffers at speeds comparable to the trigger rate, the system has no dead time.

Readout architecture. All the readout system is VME based. The present setup is the following:

i) A dedicated VME/VSB 68040 CPU runs the data acquisition software, which performs ADC control and reading and builds event records on a VME memory module.

ii) A VME connected workstation polls the event buffer for events, dumping them on tape.

iii) Another VME connected workstation performs the event display, either from the event buffer to monitor acquisition, or directly from the ADCs.

One step to improve the acquisition rate will be to add more dedicated CPUs that will process a portion of the digital channels. Full event reconstruction then can be left to off-line processing. This kind of architecture will also allow for independent acquisition on the different ADC subsets. In order to reduce VME bus occupation in this environment, a VSB interface is being implemented on the MANAGER. With this upgrade, every CPU will access its own ADC subset via VSB without interfering with each other, while the VME accesses will be reserved for CPUs synchronisation and event transfer to tape.

Event Imaging. The event display provides two bidimensional images, one for each wire plane. The two coordinates of one view are proportional to the wire number and to the drift time respectively. Each line, corresponding to a channel, reports the charge induced on the sense wire as a function of time. The sampled charge value is given as the pixel shade, the darker the pixel the higher the charge. Fig. 16 shows an example of the resulting image in the collection view. The shape of the signal corresponding to a track is approximately a step function, giving a bad looking image. Appropriate operations of filtering must be applied. An eventual three dimensional reconstruction will be based on

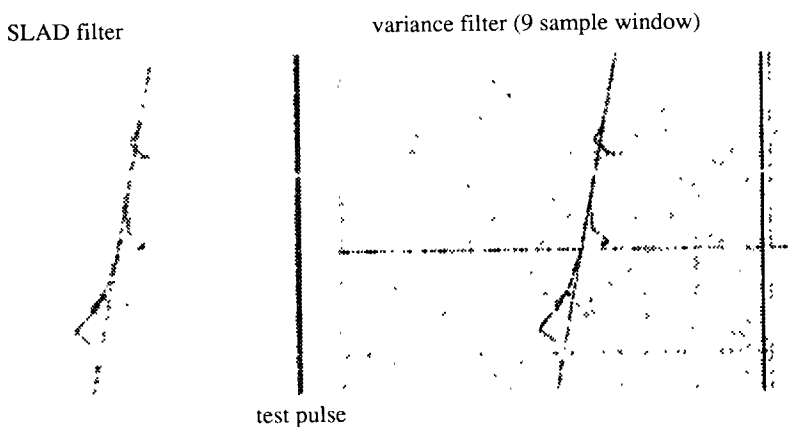

Fig. 18. Image of fig. 16 after SLAD (left) and variance (right) filtering filtering. One noisy channel is visible in the variance filtered image.

the association of signals occurring at the same time on both wire planes. Ambiguities are possible and could be resolved either by charge consistency or by introducing more induction planes.

Data filtering. Two different approaches were followed when developing the off-line processing algorithms:

1) A quick procedure was needed to improve event display during the visual scanning activity. The collection signal must be differentiated and the low frequency noise, mainly due to microphonic pickup, must be reduced as much as possible.

2) Off-line analysis requires a non biased signal extraction. This in turn implies enhancement of signal to noise ratio and reduction of baseline fluctuations.

A good solution for the first task was found with the SLAD (Shift Left And Difference) filter: the signal is delayed by an amount of time equal to the rise time duration and it is subtracted from itself. This operation doesn't affect either the rising shape or the peak height of the signal; thus the processed image data can still be used to evaluate physics parameters. The main drawback of this filter is that the noise is increased by a factor of square root of two. Due to that, the signal extraction efficiency varies with the signal height, which is not acceptable for off-line analysis. The signal from the wire passing the point marked with a rectangle in fig. 16 (where two close tracks are present) is shown in fig. 17 together with the filtered one (SLAD filtered). The SLAD filtered image is shown in fig. 18; the quality is very similar to that of bubble chamber pictures.

A more efficient algorithm, though it consumes much more CPU, matches the requirements of the second approach better and relies on the detection changes in the variance of the signal. The variance is calculated in a window whose length is comparable to the rise time duration: if no signal is present, its value will equal the noise level. The baseline value of the filter output will thus be constant. Instead, when the window starts to overlap a signal rise front, the variance will rapidly increase. The value reaches the maximum when the window completely covers the signal. The signal to noise ratio can be maximised making the window length equal to the signal rise time. Peak extraction is then simply performed by fixed threshold discrimination on the pulse height (e.g., 3 times noise variance) and pulse width. Those two parameters and the window length can be tuned to make signal extraction uniform with respect to the pulse height or to optimise the multiple track separation. Fig. 17 shows also the variance filtered signal and fig. 18 the variance filtered image; in both cases the window is 9 samples long. The efficiency and the reliability of the algorithm will be discussed elsewhere.

11. Operation and results

In this paragraph we will summarise the principal results we have reached assembling and operating the three-ton prototype liquid argon TPC. Detailed results on the measurement of the relevant physical parameters will be reported in a separate paper. We will start with a schematic chronological account of the assembly and test phases.

The final assembly of the complete system, including the wire chambers, the argon purification system, the recirculation system and the read-out electronics begun in January 1991 and was completed in May.

We started with a preliminary filling of the detector with ultra pure argon to verify:

1) The reliability of the mechanics (wire chambers, feedthroughs, electric contacts) under thermal stress.

2) The LAr purity level reachable in large volumes for a high gas flow through the purifier.

3) The reliability, the efficiency of the recirculation system and the consumption of LAr.

The liquefaction process was performed in a few steps. (a) Cleaning of all the detector pieces in solvents and demineralised water as described in section 4. (b) Evacuation of the dewar down to 10^{-7} mbar and bake-out at 90°C for 15 days. (c) Cooling down to LAr temperature using pure argon gas to uniformly thermalize the detector for 7 days. (d) Liquefaction of commercial liquid argon into the experimental dewar passed through Oxisorb and molecular sieves at a speed of 8 l per hour as described in section 6. The results concerning the LAr purity were very satisfactory. The electron lifetime measured with the internal purity monitor (described in section 6) was higher than 3 ms in 300 l of LAr liquefied at a speed of 8 l per hour. It was stable under the action of the recirculation system (running at a speed of 4 l per hour).

The purity of the gas phase on top of the liquid was also measured by condensing a small fraction of it into the external purity monitor. The resulting 100 μs electron lifetime, very different from the lifetime in the liquid phase, strongly supports the hypothesis that most of the impurity is produced by outgassing from the warmer surfaces (dewar walls and kapton cables) in contact with the gas phase and perhaps by small leaks from the more then 2000 feedthroughs. The recirculation system acts efficiently against this process because it extracts the gas phase at the top of the detector, purifies it and recondenses it back at the bottom of the dewar.

Serious problems were found concerning the wire chambers. A Macor bar on one of the two chambers broke under the mechanical and thermal stresses. A few wires (about 10 out of more then 8000) of the collection plane of the other chamber lost their tension

during cooling down to LAr temperature due to bad clamping of the copper pins. This implied that, by applying the voltage on them, short circuits were found between wire planes due to electrostatic attraction. This in turn made it impossible to continue the test.

The LAr was evacuated in five days and the detector was brought back to room temperature. The wire chambers were extracted: the one with the broken MACOR was no longer usable and on the other chamber the faulted wires were cut away. We placed in front of the unusable chamber a small chamber that we had previously used in the small scale tests with the same geometry as the large chambers. The two coordinate planes had 32 sense-wires, each 8 cm long.

The actual filling was started in April. It took 16 days to fill the dewar with 2000 l of purified LAr. The electron lifetime was continually monitored: it was about 1 ms at the beginning, increasing steadily during liquefaction and reaching a stable value of about 3 ms at the end due to the presence of the recirculation system. A test was done by stopping the recirculation system. The lifetime immediately dropped down to less than 1 ms within 4 h. Restoration of the purity was achieved in 12 hours by reactivating the recirculation system. No major defects were found on the wire chamber except a short-circuit on some screen wires of the induction plane. This had the only effect of limiting the electric field applicable to the drift region to 700 V/cm.

As a next step we started connecting the analogue electronic chain (preamplifiers, HV, decoupling capacitors, test capacitors) onto the signal feedthroughs at one end and the digital boards at the other. The implementation of the complete data acquisition chain for the 272 channels that were available was then completed.

At the end of June the first tracks from cosmic rays were seen on the on-line display. The detector was operative and we started to collect data. In parallel we have worked to improve various parts of the system, in particular the read-out electronics. The test capacitances have been calibrated to within a 1% accuracy and the cross talk between channels was reduced to below 2%. Software was developed to optimise the data reduction for speed and efficiency and to enhance the signal to noise ratio of images for off-line analysis (section 10).

The electron lifetime in the detector is continually recorded and controlled with the internal purity monitor: no significant change in the electron lifetime has ever been found, it fluctuates between 2.5 and 3 ms. At present we do not know if the lifetime is limited to this value because the purifier filters have reached their maximum efficiency or because the recirculation speed is too low to extract more impurities. We are building a setup where we will be able both to test other purification methods and to change the recirculation speed.

A large amount of data has been collected with the 3 ton prototype using cosmic rays and gamma rays sources to study the response of the detector to a wide range of energies (from a few MeV to several GeV). In the data taking we have used two main triggers, one for cosmic rays events (non contained events) and one for events from the source (contained events). The trigger for non-contained events was made up of three scintillators placed two on the top and one on the bottom of the dewar in coincidence with the signals from two groups of 16 horizontal wires each, one group at the top and one group at the bottom of the wire chamber. The trigger for muons stopping in the detector was the same but without the lowest scintillator and with the lowest group of wires in anticoincidence. The trigger

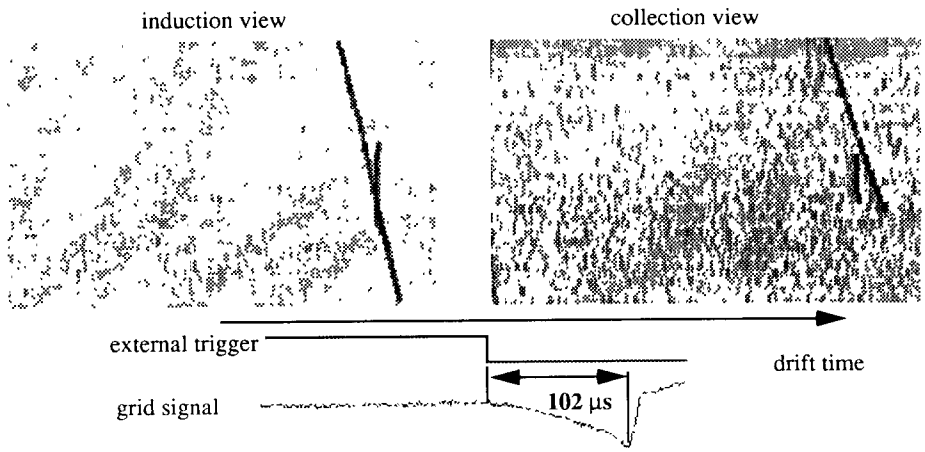

Fig 19. The two images of a cosmic ray track. Vertical heights are 32 wires with 2 mm pitch. In the lower part the external trigger and grid signal are shown.

for low energy contained events was an internal trigger built with the signals from the groups of 16 contiguous collection wires. To trigger on a region of the chamber we use an OR of the corresponding groups of wires with those at the borders in anticoincidence (to select contained events). In this way we can easily trigger down to 1 MeV in energy deposition.

Fig. 19 shows one of the first events we collected with the small chamber; it is a cosmic ray (that is probably a muon) crossing the detector triggered by the external counters in delayed coincidence with the grid signal of the chamber. The track crosses the detector almost parallel to the wire planes (drift times almost constant) at about 45° with the directions of the wires (images in the two views are very similar). The two views *xz* (induction) and *yz* (collection) are shown. As can be seen, the images are very neat: the S/N is 6 in the induction plane, 10 in the collection plane as expected with an ENC $\approx$ 1000 electrons. The electric field intensity was 330 V/cm corresponding to a drift speed of 1.35 mm/μs; the clock of the FADC was set to a 200 ns period; one pixel is then 2×0.27 mm^2, but the two scales of the figure are the same (each frame corresponds to 71 mm horizontally and 62 mm vertically).

The signal induced on the screening grid (7×8 cm^2, all wires connected together) is fed to an integrating amplifier. In the lower part of the figure the charge signal from the screen grid is shown together with the logic signal from the external trigger (the external $t = 0$). The signal from the screen grid grows initially very slowly, when the charge is still far away and the solid angle under which it sees the grid is small and slowly varying. When the charge crosses the grid the current inverts and becomes larger in value: the charges are now crossing the narrow (2 mm) gap between the screen and the induction plane and the fraction of the electric flux of the charge field collected by the screen varies rapidly (fast signal).

The fast signal is proportional to the inducing charge and, hence, to the energy deposited. In the present case this is the energy released by a minimum ionising particle in 6 cm, that is 13.2 MeV. As can be seen in the figure the noise is at a very low level. An important piece of information that can be extracted from the screen grid signal is the event time ($t = 0$). In the present case we know the time of the event from the external trigger; if we do not know it (as for contained events) we can evaluate the instant when the signal becomes different from the base line. In the example this can be done rather precisely, within a few microseconds (corresponding to an uncertainty in the absolute event position of a few mm). Unfortunately, the situation is more difficult for more complicated events (with tracks at different angles) and for larger area grids (with increased noise), but the example shows that the induced signal on suitably designed electrodes can be used in a physics experiment for $t = 0$ information (an alternative that is obvious in theory but not in practice is using the scintillation

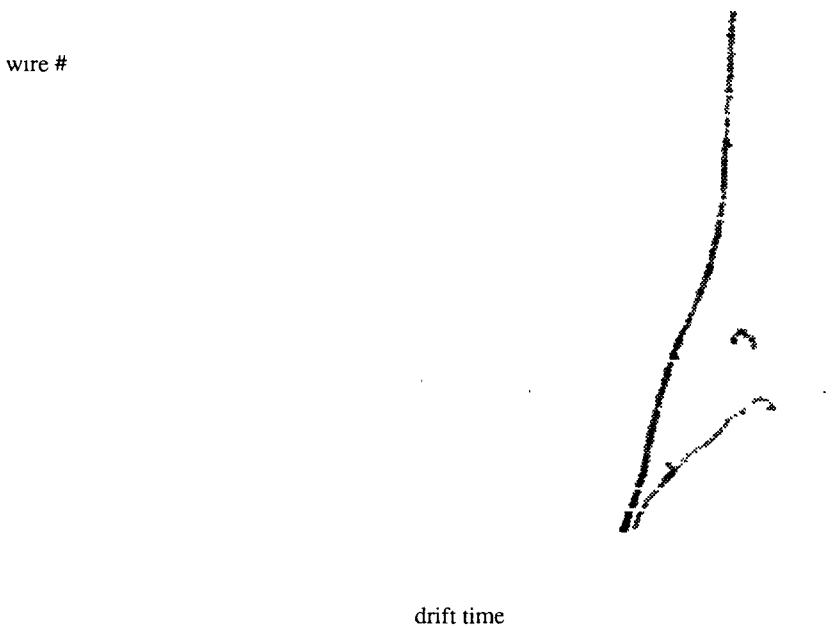

Fig. 20. A stopping muon and decay electron tracks. Collection view. The dimensions of the image are approximately 40×40 cm^2. The gap between muon and electron tracks is due to the 3 μs long life of the muon.

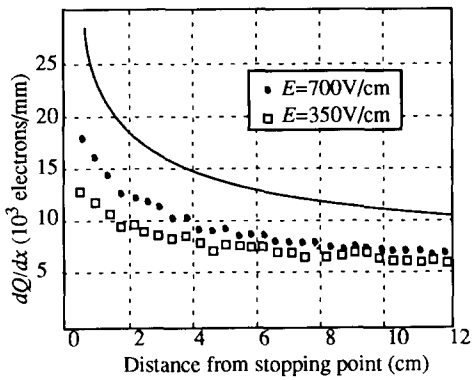

Fig. 21. Average collected charge as a function of the distance from the end point of stopping muons. Curve is the result of a Monte Carlo calculation not including recombination.

light). Further R&D work is necessary and under way on this point.

Fig. 20 shows the collection view in the large chamber of a stopping muon and of the decay electron (32 MeV energy). Again the quality of the image (approximately 40×40 cm^2 wide) is of bubble chamber grade. The separation between the electron and muon track is due to the 3 μs long muon lifetime. The grey level of the pixels codes the pulse height, proportional to the collected charge. The increase in ionisation near the stopping point is easily noticed. For contained events with a track stopping in the detector without decay or decaying without visible products, the increase of the ionisation yields the direction of the track.

Fig. 21 is a plot of the average collected charge vs. the distance from the end point for samples of stopping muons at two different electric field intensities. The increase near the end point is clearly visible. Notice that the collected charge is not proportional to that delivered by the ionising particle (Birk's law); at higher values of dE/dx the recombination is more important especially at low field intensities. The effect is visible in fig. 21 where for comparison the expected curve in absence of recombination is also shown. We are systematically analysing a high statistics sample of stopping muons to study the recombination process.

As a further example we show in fig. 22 the collection view of an electromagnetic shower. Very fine details of the event are noticeable; the shower contains both an electromagnetic and a hadronic component; a stopping muon and the decay electron are also visible. In particular, the small black dots are not noise but part of the real events; they are due to gammas with energy around 1 MeV.

Electron lifetime. The electron liftime value given by the purity monitor has been checked by means of cosmic ray muons vertically crossing the drift volume. The events have been selected requiring that there was no evidence of large multiple scattering or delta rays ensuring that they were minimum ionising particles.

The distribution of the charge deposited along the tracks is measured for each drift time slice with a binning of 20 μs; the most probable value is extracted and plotted as a function of the drift time as shown in fig. 23. An exponential fit to this plot directly gives the free electron yield (the intercept) and the electron lifetime (the slope). The fits shown in fig. 23 give at 350

Fig. 22. Collection view of a cosmic ray induced shower

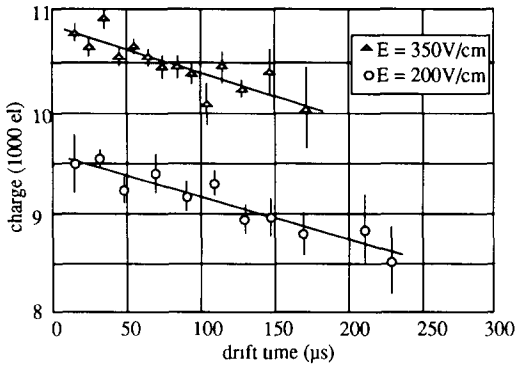

Fig. 23. Maximum collected charge per 2 mm vs drift distance for minimum ionising particles.

V/cm $\tau = 2.2 \pm 0.2$ ms for the lifetime and $Q = 10860 \pm 150$ electrons for the free charge on 2 mm and at 200 V/cm $\tau = 2.2 \pm 0.2$ ms and $Q = 9630 \pm 150$ electrons. The lifetime measurement has been repeatedly performed giving a stable value of about 2.5 ms that agrees with the data from the purity monitor.

From the analysis of through-going cosmic muons it has been already possible to extract several parameters characterising the detector: electron lifetime, free electron yield, electron diffusion, energy resolution, space resolution and particle identification capability. As for the γ-source events, the analysis is still preliminary and concerns for the time being only the self trigger capability and the energy resolution. In the future we want to exploit this source to simulate solar neutrino events to verify the reconstruction capability of the event kinematics.

Fig. 24 shows an example of a low energy event from the radioactive source. The two views of a Compton electron whose energy is about 5 MeV are shown. The trigger was the internal one described above while the electric field in the drift region was 350 V/cm. The

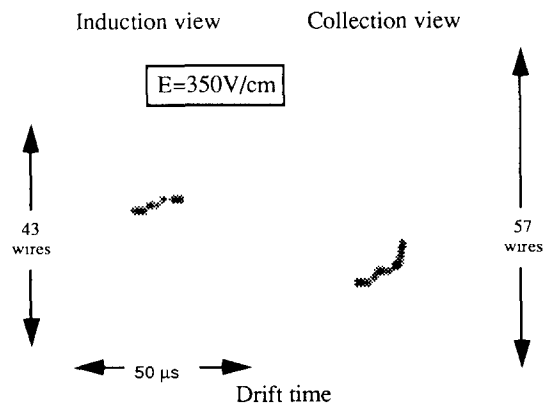

Fig. 24. The two views of a 5 MeV electron.

images are very clear particularly after noise reduction by the filtering algorithms. We are evaluating the energy resolution of the detector at low energy both by studying the fluctuation in the energy loss per unit length of minimum ionising tracks and by analysing the events from the γ-source. Spatial resolution is evaluated by studying the residuals of a linear fit for tracks of minimum ionising particles. Angular resolution for electrons with energy of some MeV, interesting for solar neutrino experiments, is under study with events from the γ-source. Detailed discussion of these results will be presented in a separate paper.

12. Conclusions

The experience with the 3 ton prototype, equipped with complex mechanical and electrical apparata immersed in the liquid and with hundreds of feedthroughs, has shown that the ultra pure liquid argon technique is reliable. Ultra pure liquid argon can be obtained using commercially available components and ultra high vacuum techniques; procedures to keep the purity in an operational detector for long periods of time have been developed and fully tested.

Three dimensional high granularity images of the ionising events have been obtained with a suitable geometry of the wire chambers. Both coherent and incoherent noises have been reduced enough to obtain good contrast images, especially after suitable filtering. Bubble chamber quality images have been obtained.

The important physical parameters of the detector, free electron yield, recombination probability, drift velocity, diffusion coefficient, free electron lifetime and their possible dependence on the electric field intensity are under study. Up to now, they are found to be in agreement with the theoretical models.

In summary we can say that a novel detector is now available for physics, even if some technical improvements are still necessary and, in fact, under way:

a) Liquid phase purification to speed up the filling of very large volumes. Recently we have succeeded in purifying commercial liquid argon in the liquid phase obtaining free electron lifetimes of several milliseconds at a rate of 500 l/h. We have not yet tested the maximum rate reachable. The results are being published elsewhere [24].

b) Doping of the liquid argon to achieve linear dependence of dE/dx on the ionisation without compromising spatial resolution.

c) Design of very large wire chambers mechanically reliable during the cool-down to LAr temperature. We have by now developed a new design of the wire chambers that foresees the construction of separate modules that will be systematically tested before being assembled.

d) Development of preamplifiers to be used immediately near the wires, i.e. in the liquid to eliminate the capacitance of the cables and to reduce the noise. We have built and tested in liquid argon some hybrid amplifiers based on a full j-FET design. The output signal is again of the current type. The ENC is very satisfactory and work is in progress to optimise layout and electrical connections.

e) Study of the best $t = 0$ system, especially optimised for solar neutrino search.

Acknowledgements

The mechanical drafting of the different components of the detector and of those used for the preliminary tests were skilfully and accurately done by M. Benvenuto. The precise work of A. Galvani and R. Pavanello in the construction of the mechanical parts has been essential, as that of J. Muffat-Jolie and M. Piffart in the wiring of the chambers.

References

[1] C. Rubbia, CERN-EP Internal Report 77-8 (1977).
[2] ICARUS collaboration, ICARUS a Proposal for the Gran Sasso Laboratory, INFN/AE-85/7 Frascati 1985.
[3] W.A. Huffman, J.M. Losecco and C. Rubbia, IEEE Trans. Nucl. Sci. NS-26 (1979) 64.
[4] H.H. Chen and J.F. Lathrop, Nucl. Instr. and Meth. 150 (1978) 585;
H.H. Chen and P.J. Doe, IEEE Trans. Nucl. Sci. NS-28 (1981) 454;
P.J. Doe, H.J. Mahler and H.H. Chen, Nucl. Instr. and Meth. 199 (1982) 639.
[5] E. Gatti et al., IEEE Trans. Nucl. Sci. NS-26 (1970) 2910.
[6] E. Buckley et al., Nucl. Instr. and Meth. A275 (1989) 364.
[7] E. Bonetti et al., Nucl. Instr. and Meth. A286 (1990)135.
[8] A. Bettini et al., Nucl. Instr. and Meth. A305 (1991)177.
[9] Oxisorb is a trade mark of Messer Griesheim GmbH.
[10] M. Miyajima, T. Takahashi, S. Konno, T. Hamada, S. Kubota, E. Shibamura and T. Doke, Phys. Rev. A9 (1974) 1438;
E. Shibamura, A. Hitachi, T. Doke, T. Takahashi, S. Kubota and M. Miyajima, Nucl. Instr. and Meth. 131 (1975) 249;
E. Aprile, W.H.M. Ku, J. Park and H. Schwartz, Nucl. Instr. and Meth. A261 (1987) 519;
E. Shibamura, Proc. JCLRD Int. Conf., p. 198 (Tokyo 1992).
[11] ICARUS collaboration, ICARUS I: An Optimized Real Time Detector of Solar Neutrinos, LNF - 89/005 (R).
[12] P. Benetti et al., Nucl. Instr. and Meth. A315 (1992) 223;
P. Benetti et al., Proc. Conf. Calorimetry in High Energy Physics (Word Scientific, 1992) p. 278;
P. Benetti et al., Proc. Dallas Conf. on High Energy Physics, 1992.
[13] The cryostat has been produced by Zanon Spa. Schio (Italy).
[14] Produced by CINEL Srl. Padova (Italy).
[15] Leybold-Heraus GmbH. Köln (Germany).
[16] MACOR is a trade mark from Corning Glass Inc.
[17] ConFlat is a trademark of Varian. USA.
[18] HYDROSORB & OXISORB type R20, Messer Griesheim GmbH, Düsseldorf, Germany.
[19] NUPRO company, Ohio, USA.
[20] VAT, Aktiengesellschaft CH-9469 Haag Switerland.
[21] V. Radeka, IEEE Trans. Nucl. Sci. NS-21 (1974) 51.
[22] C. Bacci et al., Nucl. Instr. and Meth. A273 (1988) 321; S. Centro, Nucl. Instr. and Meth. A315 (1992) 404.
[23] The digital system has been produced by CAEN Spa. Viareggio (Italy).
[24] ICARUS collaboration, to be published.